Energy Research and Development Division

FINAL PROJECT REPORT

Solar-Reflective "Cool" Walls: Benefits, Technologies, and Implementation

Appendix K: Evaluation of Self-cleaning and De-polluting Photocatalytic Wall Materials (Task 4.3 Report)

California Energy Commission
Gavin Newsom, Governor

April 2019 | CEC-500-2019-040-APK

Appendix K:
Evaluation of self-cleaning and de-polluting photocatalytic wall materials (Task 4.3 report)

Xiaochen Tang[1,2], Sharon Chen[1], Marion Russell[2], Haley Gilbert[1], Sébastien Houzé de l'Aulnoit[1], Ronnen Levinson[1], and Hugo Destaillats[1,2]

[1] Heat Island Group, Lawrence Berkeley National Laboratory

[2] Indoor Environment Group, Lawrence Berkeley National Laboratory

31 May 2018

Abstract

Photocatalytic self-cleaning materials were exposed vertically facing west for two years in three California sites. Specimens were retrieved quarterly for laboratory testing. Another set of the same materials are being exposed at other three sites in Florida, Ohio and Arizona, used for roofing rating over a period of five years, with annual retrievals. In all cases, photocatalytic materials were exposed side-by-side with non-photoactive control specimens. Photocatalytic materials exposed in California showed an excellent self-cleaning performance during all seasons. By contrast, the control material was soiled during the dry season. Photocatalytic materials also showed de-pollution effects that were sensitive to location and weather. Experiments showed nitric oxide (NO) removal and net deposition of nitrogen oxides (NO_x = NO + NO_2) in most locations and weather conditions, with fluctuations associated with atmospheric deposition and precipitation.

1 Introduction

The main goal of this task was to assess the performance of photocatalytic cool wall technologies. This was achieved by exposing these materials to the environment over a 2-year period, measuring the initial solar reflectance and its changes as a function of time. Protocols developed for the evaluation of these radiative properties have been described on the Task 4.1 Report. Specimens used in these measurements were weathered alongside the other wall products described in Task 4.2 at three locations in California: Berkeley, Los Angeles, and

Fresno. In addition, specimens were also exposed at the three sites used nationally for roofing product rating, in Florida, Arizona, and Ohio.

Photocatalytic self-cleaning products can remove soiling from their surface by catalyzing the elimination of deposited soiling in the presence of sunlight, and/or facilitating water runoff due to enhanced surface hydrophilicity. These two phenomena are illustrated in Figure 1A. Photoactive building envelope materials represent a growing sector of the construction market, with $740M in sales in 2009, doubling by 2014 (Gagliardi, 2010). These products are used in new construction and in retrofits, and include cementitious coatings such as mortar, plaster and paint; coated metal siding; architectural fabrics; tiles; precast panels; and roofing.

When these materials are exposed to sun light, photo-induced chemical processes can eliminate soiling and air pollutants adsorbed on the catalyst surface, including organic compounds and atmospheric nitrogen oxides (NO_x), as illustrated in Figure 1-B (Hoffmann et al., 1995). In the case of NO_x, photocatalytic oxidation enables a net removal of these species from the atmosphere through their irreversible conversion to the non-volatile oxidation byproducts nitrate (NO_3^-) and HNO_3. The final stable oxidation byproducts can be washed off the surface by rain or dew. Different test methods have been developed to evaluate the air purification efficiency of photocatalytic materials (Dillert et al, 2012; Mills et al, 2012; Minero et al, 2013). In this study, we adopted a commonly used approach, the ISO Standard 22197-1 “Fine ceramics (advanced ceramics, advanced technical ceramics) – test method for air-purification performance of semiconducting photocatalytic materials. Part 1. Removal of nitric oxide” (ISO, 2007).

The self-cleaning and de-polluting properties of photoactive surfaces have been documented primarily via laboratory tests. One important goal of this study is to quantify these phenomena under real-world conditions. A key barrier to the development of photocatalytic products has been the lack of metrics and methods to evaluate their performance. This study contributes with metrics and processes to facilitate the evaluation and rating of photocatalytic building envelope products.

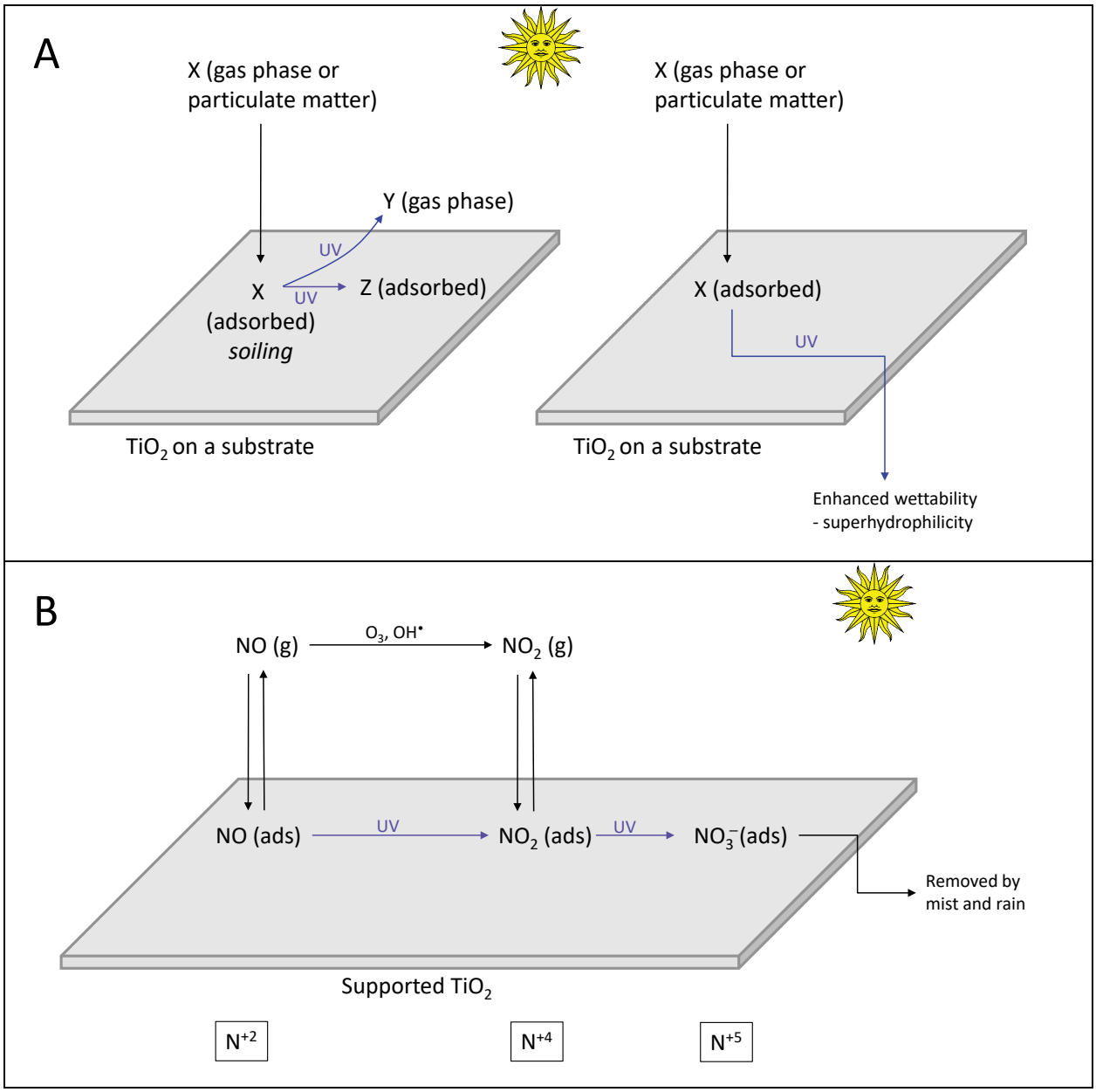

Figure 1. Illustration of (A) the self-cleaning process, and (B) the de-pollution effect of photocatalytic surfaces exposed to sun light.

2 Methodology

2.1 Selection of exposed materials

During the initial phase of the project, industrial partners were invited to submit specimens of products of interest, including specifically those that have photocatalytic additives or constituents. Despite significant efforts on our side, only two manufacturers submitted photocatalytic products. One provided photocatalytic field-applied coatings (paints); the other, architectural fabrics.

In each case, photocatalytic materials were submitted alongside their matching control samples, which were essentially products with the same characteristics but that did not have the photocatalytic functionality. Table 1 summarizes the two groups of materials, and Table 2 lists the main characteristics of each individual material. The nomenclature used in this report is the same described in Task 4.2 Report:

a) **CWXX** anonymously identifies each of the materials (where "CW" = cool walls)

b) **BK** = Berkeley, CA; **LA** = Los Angeles, CA; **FR** = Fresno, CA; **AZ** = New River, AZ; **FL** = Miami, FL; **OH** = Medina, OH.

Table 1. Summary of materials exposed in this study.

Product category	Substrate	Number of samples		Colors	Surface description
		Control	Photocatalytic		
Field-applied coating	Metal	4	4	Tan, dark green, peach	Flat
Architectural membrane	N/A	1	2	White	Textured

The photocatalytic field-applied coating samples did not exhibit de-pollution activity. Solar reflectance changes observed in those samples were attributed primarily to color changes due to bleaching, rather than soiling removal. The latter phenomenon is described in Task 4.2 Report, under section # 3.2.3 (Color changes due to product aging). For these reasons, those samples were not further evaluated in this task. Instead, this report has focused on photocatalytic architectural fabrics, which exhibited measurable de-pollution and self-cleaning performances.

Table 2. Description of materials used in natural exposure tests.

ID	Product category	Details	Commercial or experimental?	Surface sheen	Color	Substrate
CW16	coating (field)	control for CW17	experimental	flat	tan	metal
CW17	coating (field)	photocatalytic	experimental	flat	tan	metal
CW18	coating (field)	control for CW19	experimental	flat	dark green	metal
CW19	coating (field)	photocatalytic	experimental	flat	dark green	metal
CW20	coating (field)	control for CW21	experimental	flat	peach	metal
CW21	coating (field)	photocatalytic	experimental	flat	peach	metal
CW22	coating (field)	control for CW23	experimental	flat	tan	metal
CW23	coating (field)	photocatalytic	experimental	flat	tan	metal
CW24	architectural membrane	Teflon-coated fiberglass, control for CW25/26	commercial	N/A	white	N/A
CW25	architectural membrane	photocatalytic	commercial	N/A	white	N/A
CW26	architectural membrane	photocatalytic	experimental	N/A	white	N/A

2.2 Selection and setup of exposure sites

2.2.1 California sites

Three sites were selected in the State of California to expose wall materials, including the photocatalytic products and their control specimens:

a) a roof at the Lawrence Berkeley National Laboratory in Berkeley,

b) a parking lot at the University of Southern California, in downtown Los Angeles; and

c) a ground-level cement structure belonging to one of our industry partners in Fresno.

The Berkeley site was cleanest, because the Laboratory is located in a hill overlooking the San Francisco Bay Area, far from highways and heavy traffic. The Los Angeles site was representative of pollution found at a large mega-city. The Fresno site provided mostly exposure to air pollutants associated with agricultural activity, typical of the Central Valley.

Specimen holders at the three California sites were built between March and April 2016, and specimens from 69 different materials were installed immediately after their construction. Those specimens included those corresponding to the architectural fabric samples, CW24, CW25 and CW26. Specimens have been retrieved quarterly, following the schedule presented in Table 3.

Table 3. Experimental schedule for California exposure.

Site	installed	3 mo	6 mo	9 mo	12 mo	15 mo	18 mo	21 mo	24 mo
BK	Mar 2016	Jul 2016	Oct 2016	Jan 2017	Apr 2017	Jul 2017	Oct 2017	Jan 2018	Apr 2018
LA	Apr 2016	Jul 2016	Oct 2016	Jan 2017	Apr 2017	Jul 2017	Oct 2017	Jan 2018	Apr 2018
FR	Mar 2016	Jun 2016	Oct 2016	Dec 2017	Apr 2017	Jul 2017	Oct 2017	Jan 2018	May 2018

2.2.2 Exposure racks

Specimens were exposed facing west vertically (90˚ tilt) using racks specially built for this purpose. The design and construction of the racks was described in the Task 4.2 report: *Natural exposure of wall products*.

Figure 2A illustrates two of the three racks used in the Berkeley site. Figure 2B shows a photo of an individual architectural fabric specimen. Given the flexibility of this material, it was very important to keep it secured against the wood backing by clamping on the top and bottom sections.

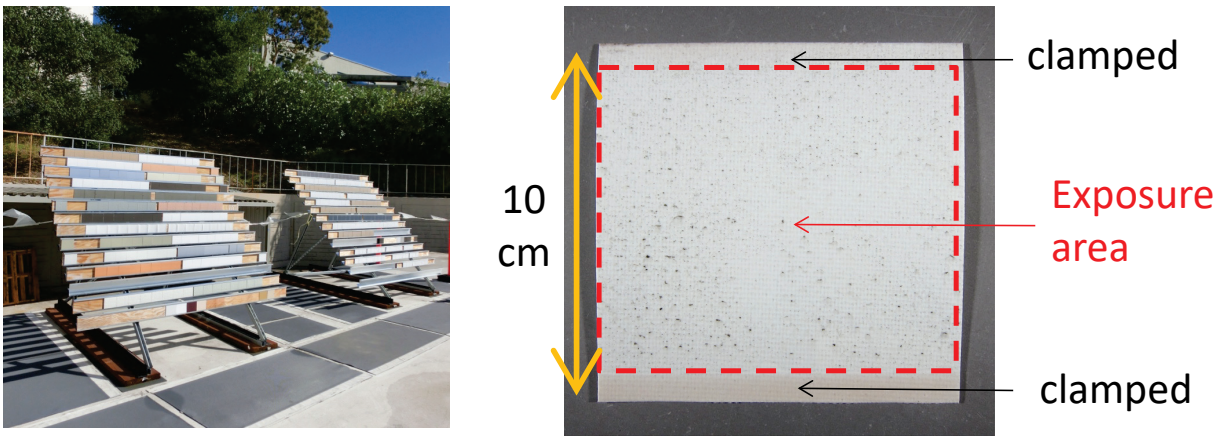

Figure 2. Exposure racks used in this study, and example of one architectural fabric specimen.

2.2.3. National exposure

In addition to the California sites, the project scope was expanded to include also the three sites used by the Cool Roof Rating Council for roofing rating. These "U.S." sites were located in New River, AZ; Miami, FL; and Medina, OH. They were operated by a commercial weathering firm that uses west-facing vertical racks. U.S. national exposure was initiated on August 2016 and is schedule to run for five years, with annual specimen retrievals each summer following the schedule presented in Table 4.

Table 4. Experimental schedule for national exposure.

Site	installed	1 yr	2 yr[a]	3 yr[a]	4 yr[a]	5 yr[a]
AZ	Aug 2016	Aug 2017	Aug 2018	Aug 2019	Aug 2020	Aug 2021
FL	Aug 2016	Aug 2017	Aug 2018	Aug 2019	Aug 2020	Aug 2021
OH	Aug 2016	Aug 2017	Aug 2018	Aug 2019	Aug 2020	Aug 2021

[a] Pending at the time this report was prepared.

2.2.4. Rainfall at each site

Monthly rainfall data at each exposure site was obtained from nearby Global Historical Climatology Network (GHCN) weather stations. The data sets were downloaded from the National Oceanic and Atmospheric Administration (NOAA, 2018). The weather stations selected for each site were:

a) US1CAAL0018, in Berkeley, 3.2 km southeast of the Berkeley exposure site;

b) USW00093134, on the University of Southern California (USC) campus, 1.4 km west of the Los Angeles exposure site;

c) USW00093193, at the Fresno Yosemite International Airport, 9.9 km north of the Fresno exposure site

d) US1AZMR0416, in Anthem, AZ, 3.1 km southeast of the Arizona exposure site;

e) USC00087020, in Miami, Florida, 2.5 km northeast of the Florida exposure site; and

f) US1OHMD0002, in Brunswick, OH, 16 km northeast of the Ohio exposure site.

2.3 Experimental procedures

The general experimental procedures implemented to perform measurements in the laboratory have been described in the Task 4.1 Report *Metrics and methods to assess cool wall performance*. The key measurements are highlighted in this section.

2.3.1 Specimen retrieval, shipping and storage

Photocatalytic specimens (and their controls) exposed in California were retrieved quarterly and sent back to LBNL for laboratory analysis along with the other materials exposed as part of Task 4.2. One specimen from the ten units exposed side-by-side for each material were retrieved from the racks, recorded, packed and shipped to LBNL in an individual glassine envelope. The samples were stored inside the same envelopes prior and after laboratory measurements. There was no exposure to sunlight after the specimens were retrieved from the racks.

2.3.2 Solar reflectance and spectral measurements

Solar reflectance was measured on all photocatalytic specimens and their control samples with a reflectometer (Devices & Services). The solar reflectance results are presented on the air mass 1 global horizontal (AM1GH) solar spectrum (relevant for roofs). After corrections to instrument outputs are finalized, future analyses will report the air mass 1.5 vertical (AM1.5GV) solar reflectance (relevant for walls). Per manufacturer's instructions, the solar reflectance of previously unexposed architectural fabrics was measured on specimens that had been pre-weathered in the laboratory by exposure to UV light. This step was necessary to remove a polymeric protective layer from the material surface.

2.3.3 Photography of specimens

The image of each specimen was obtained with a digital camera using a setup that provided good lighting conditions and a grey card used in the background.

2.3.4 Measurement of the de-pollution performance

2.3.4.1 Experimental setup

The experimental setup used to evaluate the de-pollution performance follows the conditions established by ISO Standard 22197-1 (ISO, 2017), and is described in

Figure 3. Laboratory air was pre-filtered with an activated carbon bed and a HEPA filter, and enriched with 1000 ppb nitric oxide (NO) prior to entering the exposure chamber. The relative humidity was adjusted to 50% by splitting the air flow and circulating one of the two flows through a water bubbler. In the exposure chamber, a specimen from either CW24, CW25 or CW26 was installed facing upwards in the center. A UV-A lamp with maximum intensity at ~360 nm (Model TL-D, Actinic BL, Philips, Andover, MA) was used to irradiate the specimen through a quartz window on the chamber's cover. The distance between the window and the specimen was 5 mm. The irradiance at 360 nm was measured using a digital radiometer (Model UVX, UVP LLC, Upland, CA). It was highest at the center of the sample and consistent over the exposed surface, with an average of 11.5 ± 1.5 W/m². The stability of the lamp during the experimental period was verified. Figure 4 shows a side view and a top view of the exposure chamber.
The chamber was kept at a constant temperature of 60 °C using an external circulating bath, to simulate conditions that are closer to those found in building surfaces under the sun. Air exiting the chamber was split into two flows; one of them was directed to a chemiluminescence NO_x analyzer (Model 200A, Teledyne Technologies, Thousand Oaks, CA), which was calibrated at different times during the entire studied period. The other chamber air stream was used to measure temperature and relative humidity prior to venting in a fume hood, using an in-line digital T/RH sensor (HIH6100 series, Honeywell),

Data acquisition was made in real time, with a resolution of ~5 seconds (frequency of 0.2 Hz). It comprised the NO and NO_2 concentrations at the reactor outlet, the air temperature and relative humidity, and the chamber temperature.

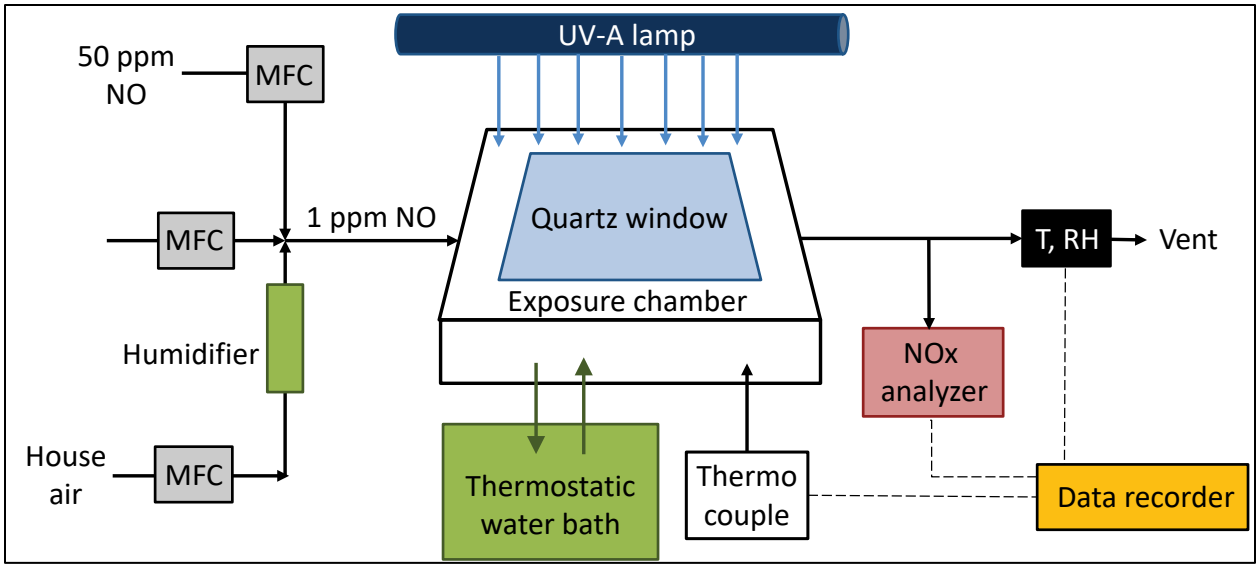

Figure 3**. Experimental setup used to evaluate the de-pollution effect**

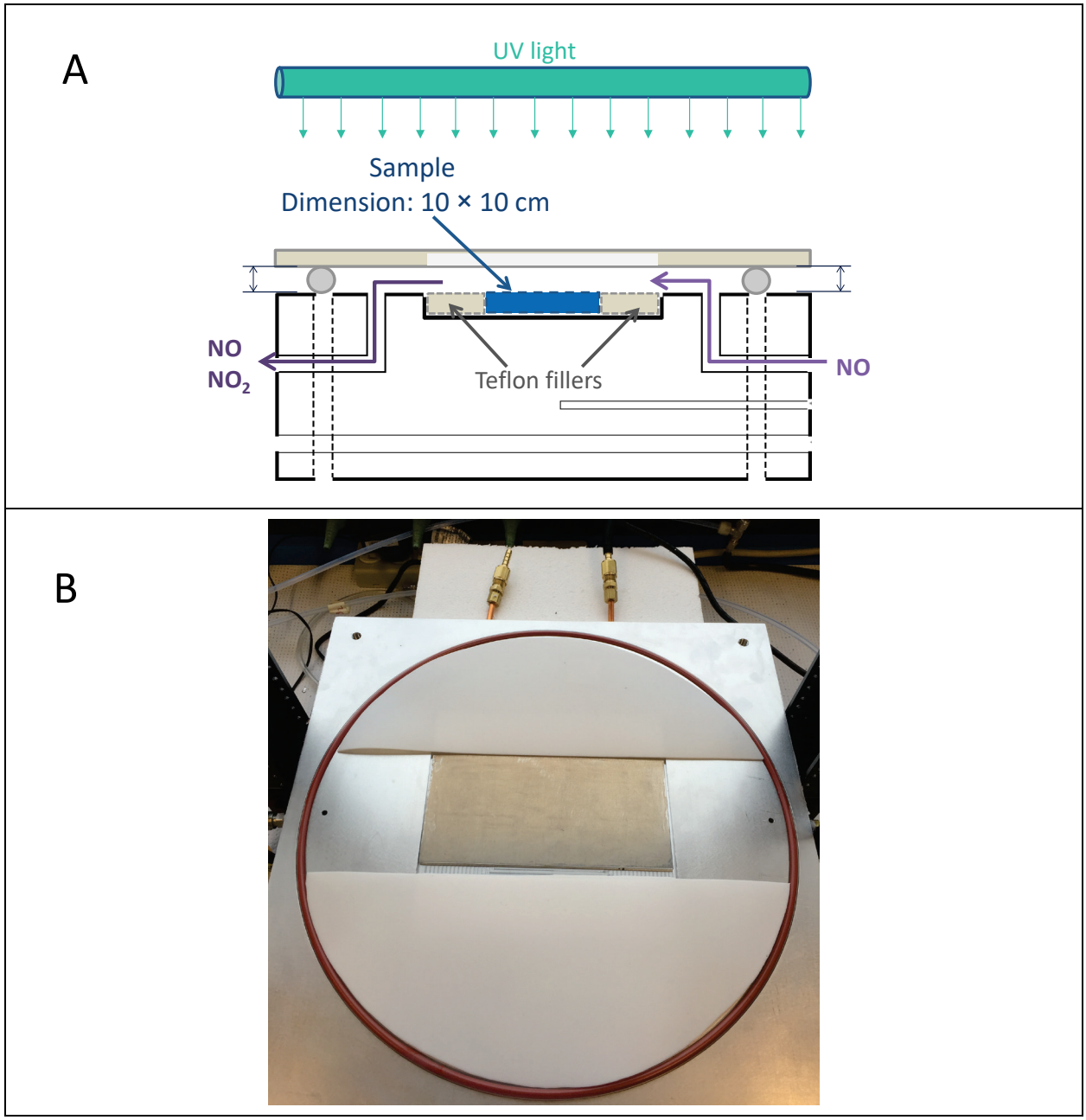

Figure 4. (A) Side view of exposure chamber; (B) Top view of exposure chamber with a reference specimen placed inside.

2.3.4.2 Experimental protocol

Tests carried out with each specimen comprised the following three segments:

a) pre-equilibration under a constant flow of NO-enriched air in the dark (~1 hour);

b) continuous UV irradiation under a constant flow of NO-enriched air (~ 6 hours), and

c) post-equilibration under a constant flow of NO-enriched air in the dark (~1 hour)

Figure 5 illustrates curves corresponding to typical NO and NO_2 traces. Removal rate of NO (r_{NO}, µmol/h) and formation rates of NO_2 (r_{NO_2}, µmol/h, from oxidation of NO) were calculated using the difference between the inlet and outlet concentrations of NO and NO_2, as follows:

$$r_{\mathrm{NO}} = \frac{\int_0^t n_{\mathrm{NO_{removed}}} dt}{t} = \frac{\int_0^t (c_{\mathrm{NO_i}} - c_{\mathrm{NO_{out}}}) dt}{t} \times \frac{Q}{V_n} \quad (1)$$

$$r_{\mathrm{NO_2}} = \frac{\int_0^t n_{\mathrm{NO_{2formed}}} dt}{t} = \frac{\int_0^t (c_{\mathrm{NO_{2out}}} - c_{\mathrm{NO_{2i}}}) dt}{t} \times \frac{Q}{V_n} \quad (2)$$

where Q and t are the flow rate and irradiation duration, and V_n is the normalized gas volume for one mole of gas at standard pressure and room temperature. This approach is illustrated in Figure 5-B. If we assume that nitrate is the only byproduct formed apart from NO_2, the rate of nitrate formation can be calculated from the difference between the values calculated with equations 1 and 2. This estimate would provide a best-case scenario prediction for the amount of nitrate that can be formed. The relative NO_2 yields (Y_{NO_2}) was determined as the ratio between the NO_2 formation rate and the NO reaction rate:

$$Y_{\mathrm{NO_2}} = \frac{r_{\mathrm{NO_2}}}{r_{\mathrm{NO}}} \quad (3)$$

The nitrate buildup rate can be predicted as the mass of nitrate formed per unit time and area ($R_{nitrate}$, mg/h· m²). Similarly, the NO_x deposition rate can be computed as the difference between NO removal and NO_2 formation rates per unit area, expressed in moles (R_{NO_x}, μmol/h·m²). The exposed surface area for each specimen was 0.01 m².

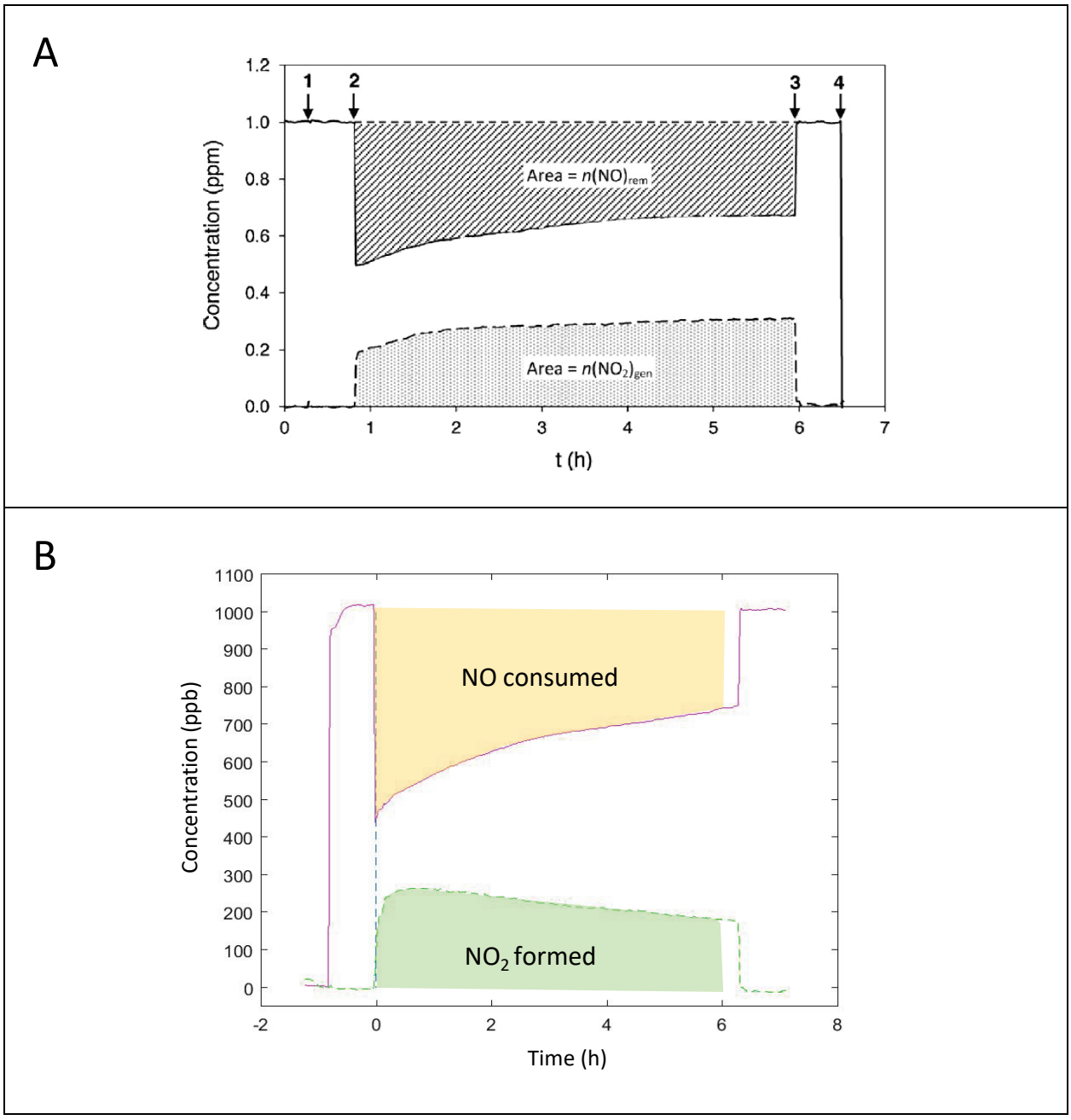

Figure 5. Examples of NO_x traces (A) adapted from Mills and Elouali (2015), and (B) recorded in this study.

3 Results and discussion

3.1 Rainfall recorded at each site

Rain patterns at the three California sites were very similar, and are presented in Figure 6. Across the State we observed a dry season from April/May to October, and a rainy season through the late fall, winter and beginning of the spring. Maximum precipitation was recorded in January 2017 in all three sites. Considering total volume of rain measured at each location, Berkeley was the site that experienced the most cumulative rainfall (approximately 160 cm through April 2018), with Los Angeles and Fresno receiving comparable lower amounts of rain (approximately 60 and 70 cm through April 2018, respectively).

One significant difference in the rain patterns was that precipitation in LA was mostly taking place during the winter months (December through February), while the other two sites showed a broader distribution, with significant levels from October through April.

3.2 Evaluation of the self-cleaning effect

3.2.1 Visual inspection

The self-cleaning effect was relatively easy to appreciate visually, as shown in the photos presented in

Figure 7. Specimens of the control material CW24 that were exposed side-by-side with the photocatalytic specimens CW25 and CW26 were much more significantly impacted by dust and soiling, leading to a visible change in color. This effect was more marked during the dry season and was significantly reduced during the rainy season.

3.2.2 Solar reflectance measurements

Measurements of solar reflectance of each specimen confirmed that, as the materials became dirtier, their albedo was reduced. Figure 9 compares the changes in solar reflectance recorded for CW25 with respect to CW24 (control). Similarly, Figure 10 makes the same comparison between the other photocatalytic product, CW26, and the control material. In both cases, the gap between photocatalytic and control materials was significant: it was higher than 0.10 at the maximum distance for specimens exposed in Los Angeles and Fresno. The gap was reduced significantly during the rainy season, in parallel to the cleaning of the control material observed visually.

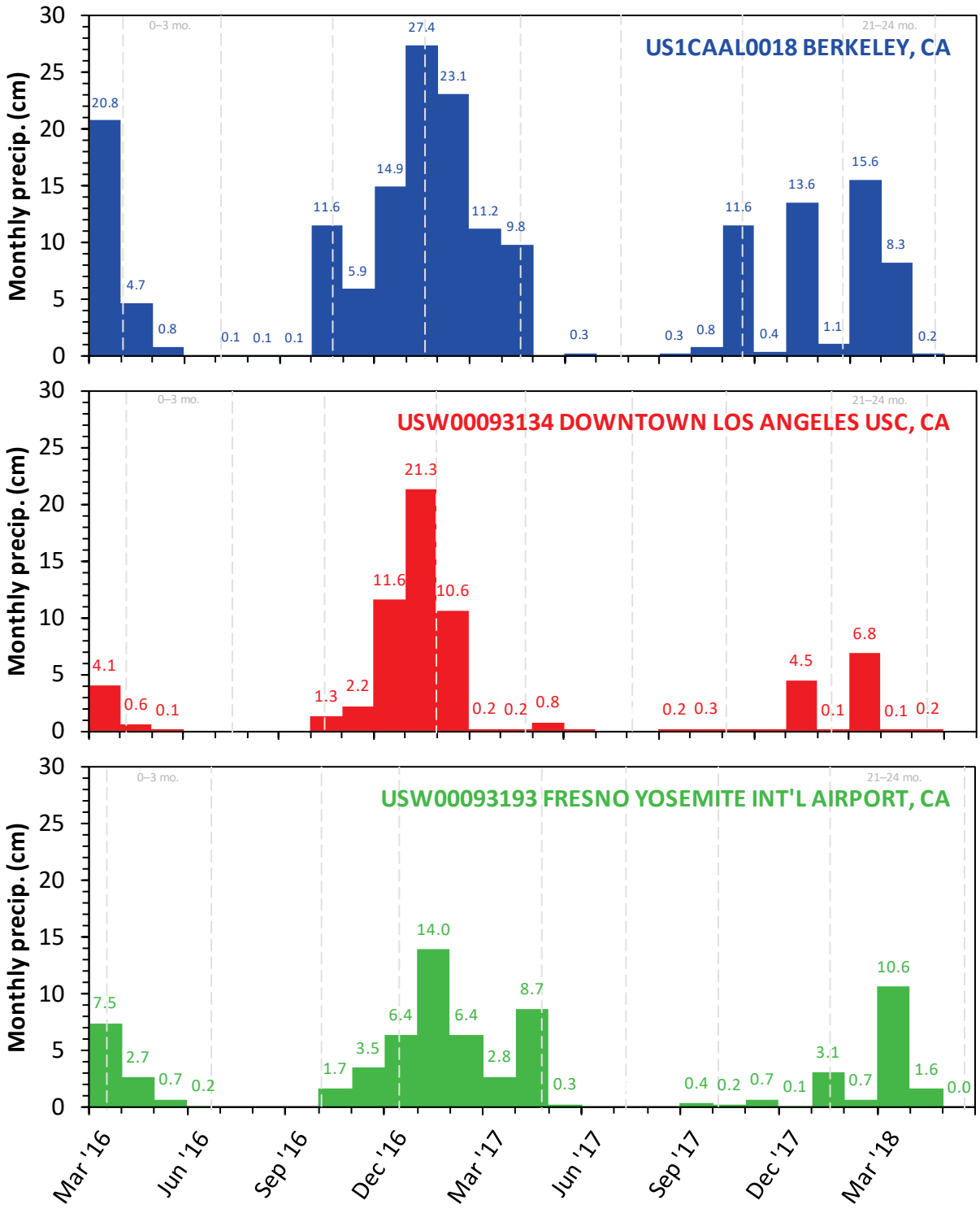

Figure 6. Rainfall patterns at the California exposure sites.

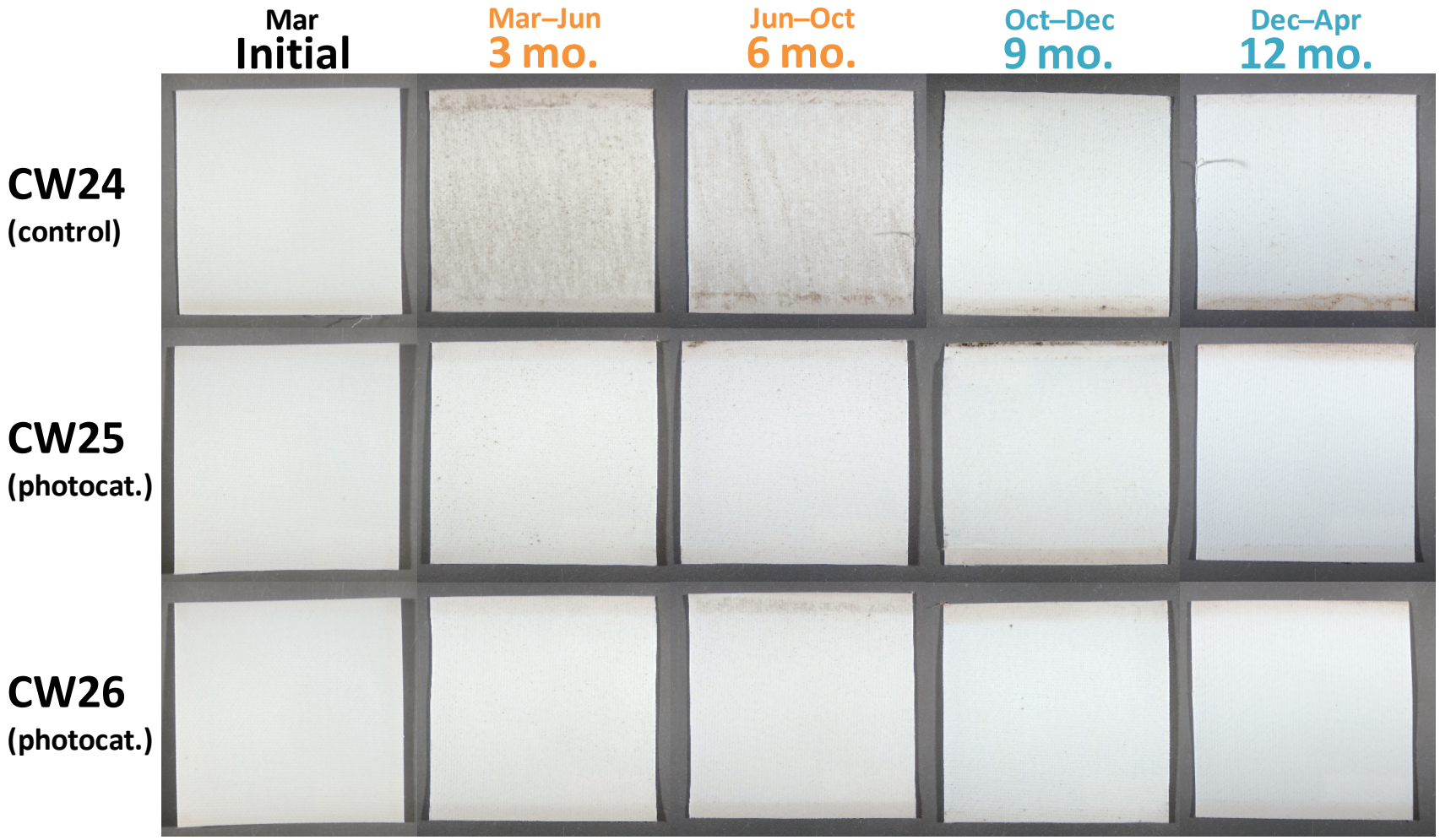

Figure 7. Images of specimens exposed in Fresno.

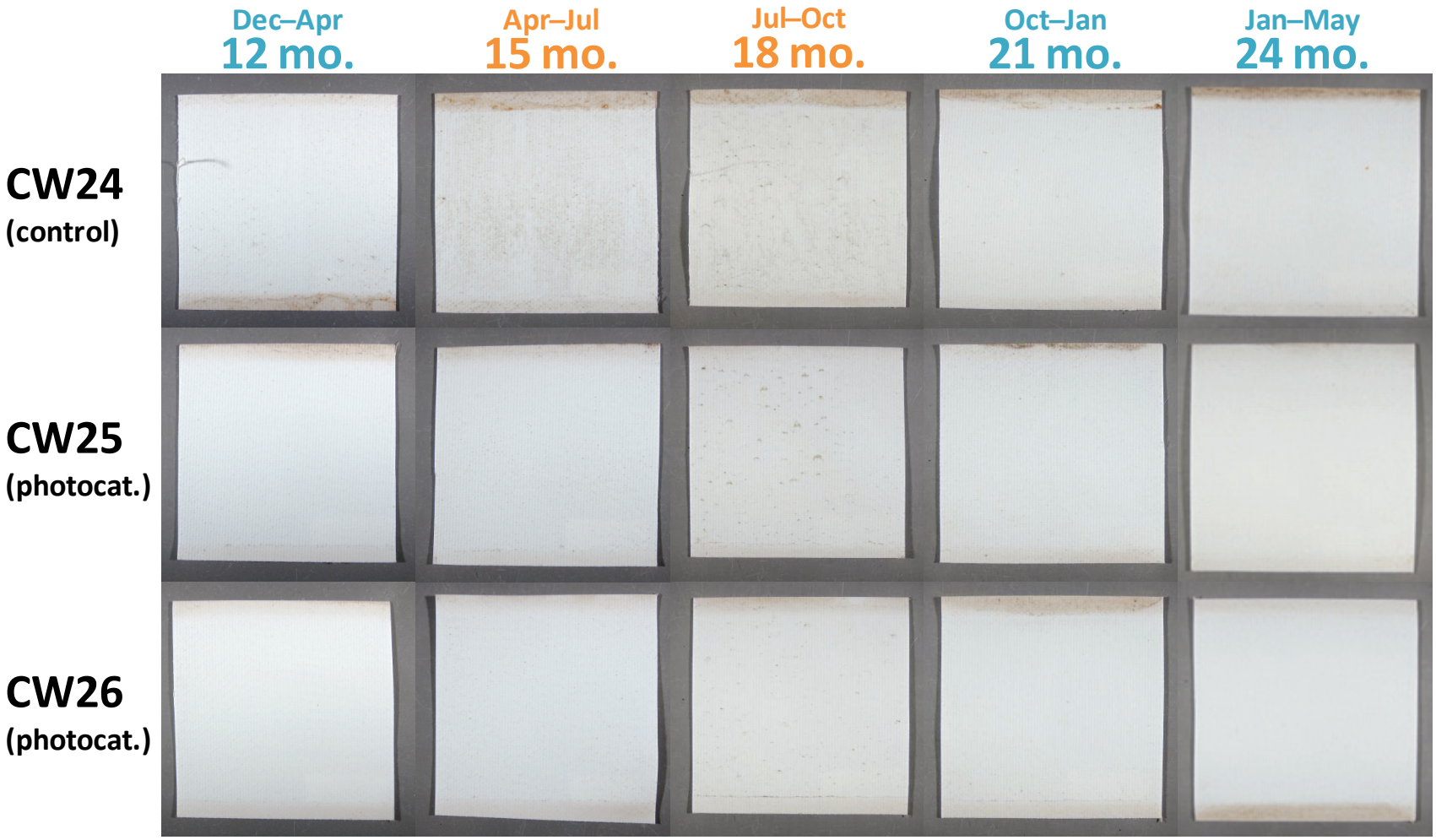

Figure 8, continued. Images of specimens exposed in Fresno.

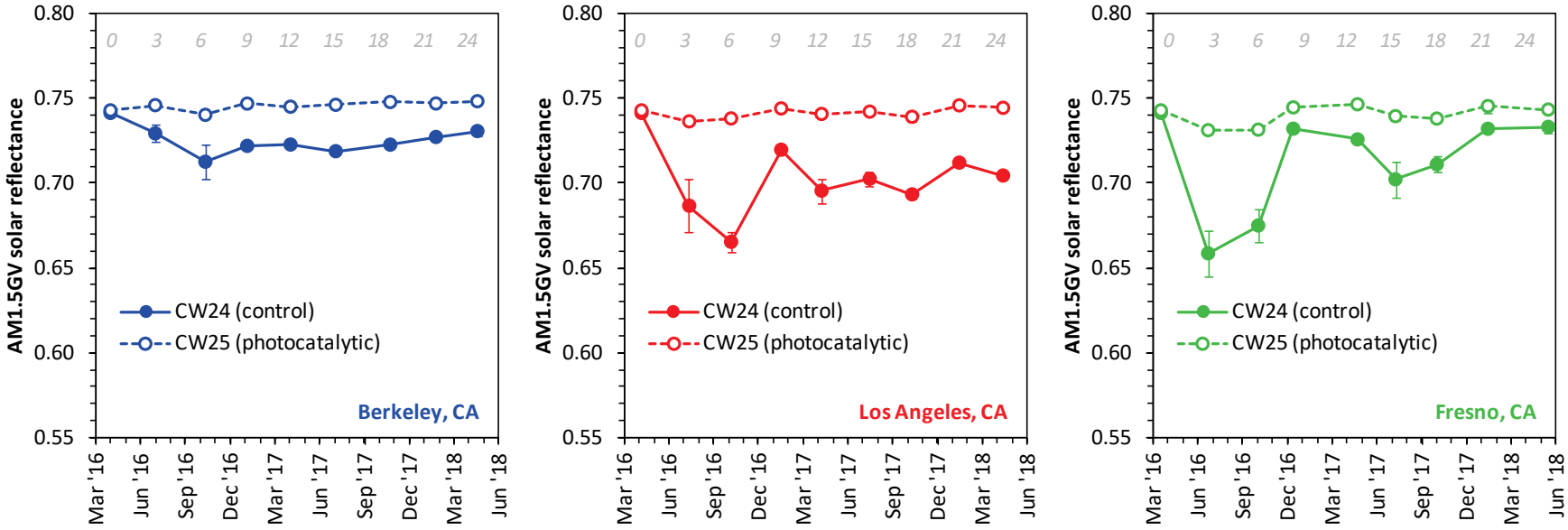

Figure 9. Solar reflectance of architectural fabrics CW24 (non-photocatalytic control) and CW25 (photocatalytic) measured in the three California sites.

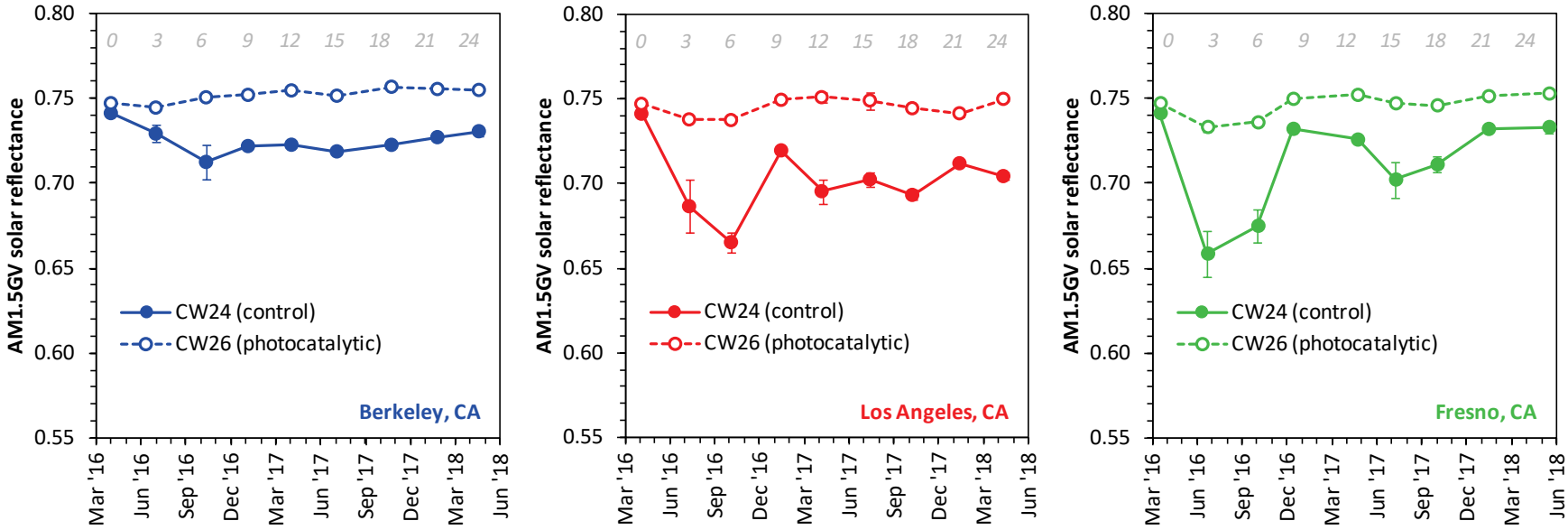

Figure 10. Solar reflectance of architectural fabrics CW24 (non-photocatalytic control) and CW26 (photocatalytic) measured in the three California sites.

3.3 Evaluation of the de-pollution effect

3.3.1 NO and NO_2 concentration profiles

Figure 11 illustrates experimental results obtained to evaluate the NO_x removal efficiency of the photocatalytic specimens and their controls. The time scale was re-zeroed at the time the UV lamp was turned on. The ~1 hour before the zero time was used to equilibrate the material with the NO_x-enriched atmosphere. When a control specimen CW24 was used, no change in NO and NO_2 concentrations was recorded, indicating that there was no reaction taking place upon irradiation alone. However, when specimens from the materials CW25 and CW26 were used, the NO and NO_2 curves showed features similar to those presented in Figure 10-B. There was an initial sharp decline in NO concentrations, accompanied by a sharp increase in NO_2 concentrations. Subsequently, NO concentrations increased asymptotically reaching a steady-state value after ~3 hours of irradiation. During the same period, NO_2 concentrations declined reaching a plateau at the same time. After six hours of irradiation, the UV lamp was turned off, and both NO and NO_2 concentrations rapidly recovered their initial values (ca. 1000 ppm and 0 ppm, respectively).

3.3.2 NO removal rates

From the integration of the curves shown in Figure 11 using equations 1 and 2, it was possible to calculate the rate of NO elimination, which is reported in Figure 12 for each specimen aged in each California site. This is the primary photocatalytic process, which leads to the formation of both NO_2 and nitrate. The material CW25 shows a significantly higher efficiency in NO elimination, as compared with CW26 in all three sites and almost all weather conditions. In Fresno and Berkeley there is a decline in performance associated with the dry season, which is reverted during the rainy season.

3.3.3 NO_x deposition rates

By subtracting the NO_2 formation rate from the NO removal rate, it was possible to determine in each case the NO_x deposition rate, which is presented in Figure 13. Overall, these rates are of lower magnitude than the primary process, the NO removal rate, due principally to the fact that a fraction of NO is converted to NO_2. However, there is a net NO_x deposition rate in most conditions. The negative values recorded in Fresno and on one occasion in Los Angeles are likely due to the presence of other nitrogen-containing species in soiling material deposited on the specimens, which can be photocatalytically converted to NO_x. This is particularly relevant for ammonia aerosols, which are commonly found in rural environments such as the one surrounding the Fresno site.

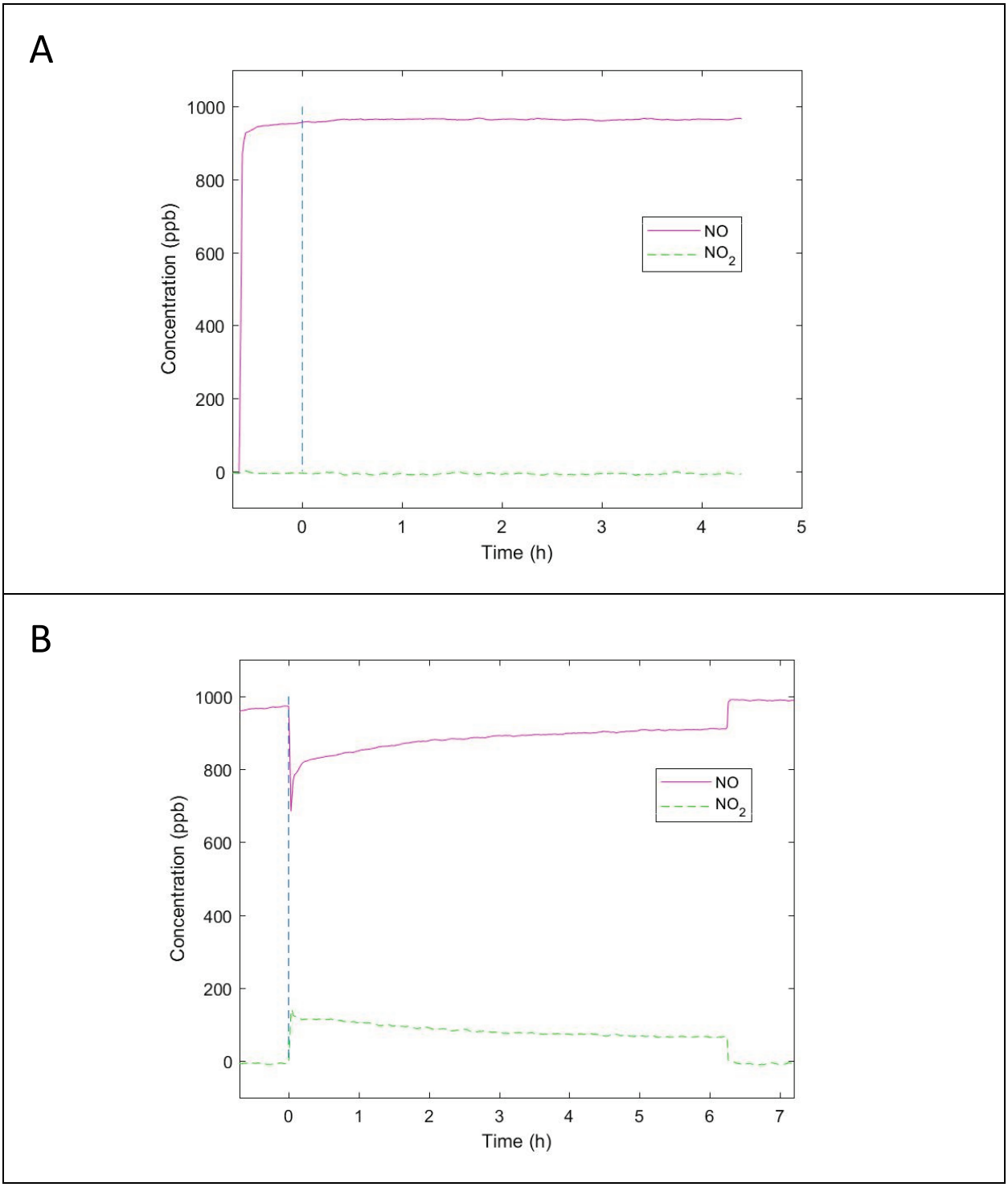

Figure 11. Typical NO and NO_2 concentration curves recorded in experiments with (A) CW24, and (B) CW25 and CW26.

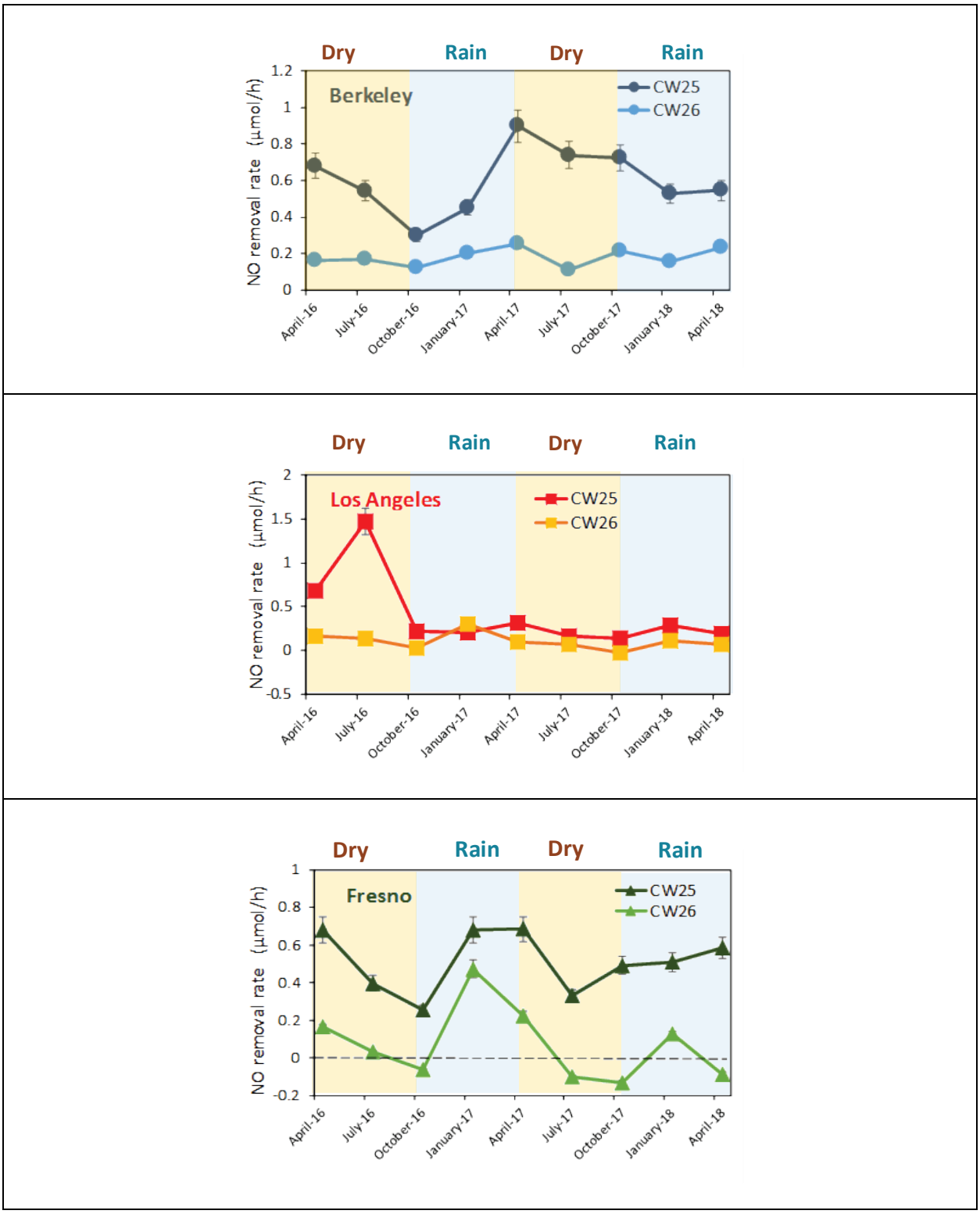

Figure 12. NO removal rate determined in each of the California sites.

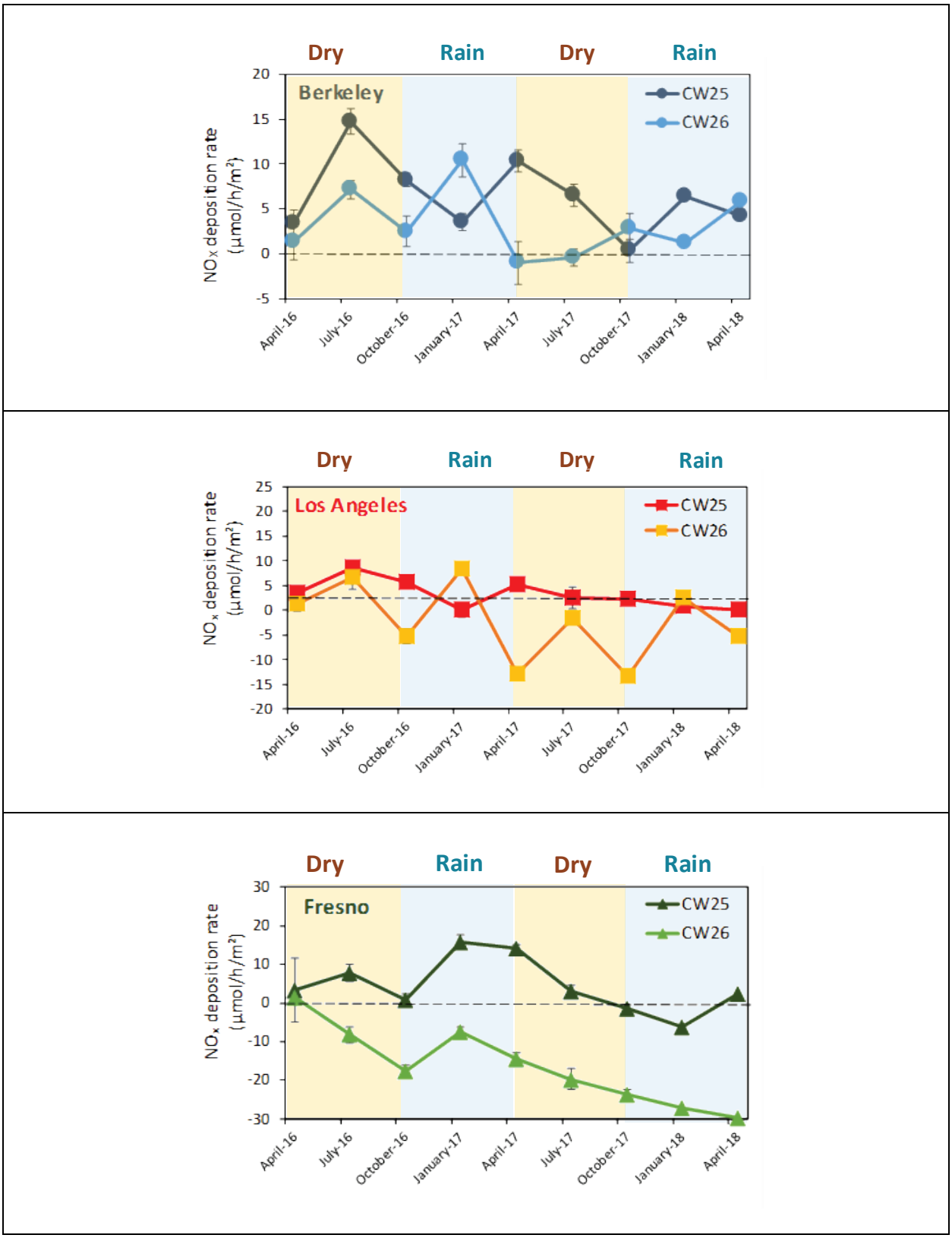

Figure 13. NO_x removal rate determined in each of the three California sites.

4 Conclusions

Results corresponding to both photocatalytic products (CW25 and CW26) show an excellent self-cleaning performance in all three California sites and during all seasons. The photocatalyst additives can successfully protect the surface from soiling buildup, preserving its original appearance.

The de-pollution effect shows a more marked effect of both location and weather. While NO removal and a net NO_x deposition were observed in most cases, there were fluctuations that were associated with the effects of atmospheric deposition and precipitation. While the materials were very effective in removing visible soiling agents, it is likely that some recalcitrant oxidation byproducts remained attached to the catalyst and may have built up over time during the dry season. Examples of those recalcitrant species are carboxylic and polycarboxylic acids, which have a low vapor pressure and are likely to remain attached to active sites, thus partially inhibiting the catalysts ability to react with NO_x and other atmospheric species. This effect can be reduced during the rainy season because while those species are not very volatile, they are water soluble and can be dissolved and removed by liquid water present on the surface.

5 Future work

The results of this project will be further systematized during the preparation of an archival journal article summarizing the key results.

National exposure is schedule to continue through 2021. We will retrieve CW24, CW25 and CW26 specimens exposed in FL, OH and AZ in August of 2018, 2019, 2020 and 2021. This information will contribute to a more complete evaluation of the self-cleaning and de-pollution performance of these materials.

References

Dillert R, Stotzner J, Engel A, Bahnemann DW. 2012. Influence of inlet concentration and lightitensity on the photocatalytic oxidation of nitrogen (II) oxide at the surface of Aeroxide ® TiO2 P25. *J. Haz. Mater.* 211, 240-246.

Gagliardi M. 2010. Photocatalysts: Technology and Global Markets. BCC Research. Available online at: https://www.bccresearch.com/market-research/advanced-materials/photocatalysts-tech-markets-avm069a.html

Hoffmann MR, Martin ST, Choi WY, Bahnemann DW. 1995. Environmental applications of semiconductor photocatalysis. *Chem. Rev.* 95, 69-96.

ISO. 2007. Fine ceramics (advanced ceramics, advanced technical ceramics) – test method for air purification performance of semiconducting photocatalytic materials. Part 1: Removal of nitric oxide. International Organization for Standardization, Standard 22187-1.

Mills A, Hill C, Robertson PKJ. 2012. Overview of the current ISO test for photocatalytic materials. *J. Photochem. Photobiol. A – Chemistry*, 237, 7-23.

Mills A, Elouali, S. 2015. The nitric oxide ISO photocatalytic reactor system: Measurement of NO_x removal activity and capacity. *J. Photochem. Photobiol. A – Chemistry* 305, 29-36.

Minero C, Bedini A, Minella M. 2013. On the standardization of the photocatalytic gas/solid tests. *Int. J. Chem. Reactor Engineering*, 11, 717.